Synthesis of Cu_2O/Ag Composite Nanocubes with Promising Photoluminescence and Photodegradation Activity over Methylene Blue Dye

K.R. Basavalingaiah[1,2], Udayabhanu[3], S. Harishkumar[3,4], G. Nagaraju[3], Chikkahanumantharayappa[1,*]

[1]*Department of Physics, Vivekananda Degree College, Bengaluru, Karnataka 560055, India*
[2]*Department of Science, Government Polytechnic, Tumkur, Karnataka 572103, India*
[3]*Energy Materials Research Laboratory, Department of Chemistry, Siddaganga Institute of Technology, Tumkur, Karnataka 572103, India*
[4]*Department of Pharmaceutical Chemistry, Kuvempu University, Post-Graduate Centre, Kadur, Karnataka 572103, India*

*Corresponding author: E-mail: chrayappa@gmail.com

Received: 17 April 2019, Revised: 04 June 2019 and Accepted: 11 June 2019

DOI: 10.5185/amlett.2019.0032
www.vbripress.com/aml

Abstract

Cu_2O and Ag-Cu_2O nanoparticles were prepared via reflux method using EDTA. From the PXRD, FTIR, UV-DRS studies the synthesized NPs were characterized. The morphologies of the prepared NPs were studied by SEM and TEM analysis. The synthesized NPs were tested for photocatalytic and photoluminescence studies. The PXRD data indicated that the synthesized nanoparticles belong to cubic phase structure and space group Pn-3m. The SEM data revealed that cube like structure were obtained. Cu_2O and Ag-Cu_2O Nps were taken for determine the photocatalytic activity study on methylene blue dye, the results indicated that Ag-Cu_2O NPs exhibited promising photocatalytic activity. This is due to occurrence of Ag particles on the Cu_2O material, which makes the catalyst more sensitive. Furthermore, a photoluminescence study reveals that Cu_2O and Ag-Cu_2O nano particles shown yellow light emission. Copyright © VBRI Press.

Keywords: EDTA, Ag-Cu_2O, Cu_2O-cubes, photocatalytic, photoluminescence.

Introduction

Industrial dyestuff contains one of the largest groups of organic compounds that lead to discoloration of water and cause great loss of aquatic life. The elimination of these colors and other organic materials is a priority for ensuring a safe and clean environment [**1**]. Over the last decades, photocatalysis has attracted special attention as an economic and environmentally safe option for solving energy and pollution problems [**2**]. Among various semiconductors showing photocatalytic activity, wide band gap semiconductors such as TiO_2, ZnO, etc. bear tremendous hope in helping ease the energy and environment crisis through effective utilization of solar energy based on photovoltaic and water-splitting devices [**3, 4**]. Unfortunately, their wide band-gaps do not allow the utilization of visible light, which limit their practical applications. Therefore, it is imperative to develop new kinds of photocatalysts with high activities under visible light in view of the efficient utilization of solar energy.

Cu_2O is one of the few p-type direct band gap semiconductors with a narrow band gap of 2.17 eV [**5**], which matches the solar visible spectrum well. With the additional advantages of nontoxicity, low cost and abundance of its starting material, Cu_2O has attracted interest as a good candidate material for photocatalytic degradation of organic pollution, such as methyl orange (MO) [**6, 7**], brilliant red X-3B, [**8**] and methylene blue etc. However, previous reports indicated that Cu_2O usually exhibited low photocatalytic activity [**9, 10**], and could be deactivated by photo corrosion [**11**]. Aravind, *et al.* [**12**] the preparation for Cu_2O/Ag nanocomposite (NPs) using ethylene glycol under microwave irradiation within a short duration of time the catalytic application of Cu_2O/Ag NPs for the synthesis of substituted pyrroles via multicomponent reaction (MCRs) by using an aldehyde, amine, 1,3-diketone and nitromethane at room temperature. Zhenghua *et al.* [**13**] Ag/Cu_2O heterogeneous nanocrystals are successfully prepared by depositing

noble metal nanoparticles onto the surfaces of Cu_2O octahedral nanocrystals through a simple photocatalytic process. The photocatalytic properties of the prepared Ag/Cu_2O heterogeneous nanocrystals are studied, showing enhanced photocatalytic activities. Wang *et al.* [**14**] employ a facile and novel route to synthesize $Ag\text{-}Cu_2O$ nanocomposite films through the self-assembly of nanoparticles at an air-liquid interface. In the ethanol-water phase, $AgNO_3$ and $Cu(NO_3)_2$ were reduced to $Ag\text{-}Cu_2O$ nanoparticles by $NaBH_4$ in the presence of cinnamic acid. A K Sasmal, *et al.* [**15**] Cu_2O–Ag has been found to exhibit excellent anionic dye adsorption properties together with organic transformation for effective water remediation. Cu_2O–Ag was prepared through a facile but controlled galvanic reaction between cuprous oxide (Cu_2O) and silver nitrate ($AgNO_3$), rendering stability and porosity. The experimental results of adsorption showed that Cu_2O–Ag bears an exceptionally high adsorption capacity toward methyl orange (501.23 mg g^{-1}), which is higher than most reported results. Weixin, *et al.* [**16**] Cu_2O/Ag composite nanospheres (CNSs) with tunable Ag coverage and optical properties have been prepared based on a one-pot room temperature method by adding $AgNO_3$ solution to fresh Cu_2O nanosphere-produced mother solution in various ratios. The photocatalytic activity enhanced. Jianbo, *et al.* [**17**] $Ag–Cu_2O$ nanocomposites were synthesized via a wet-chemical precipitation route. The photocatalytic property was studied upon simulated sunlight. Enhanced photocatalytic property of $Ag–Cu_2O$ composites, compared to pure Cu_2O particles. Yangang, *et al.* [**18**] a facile solution deposition method has been demonstrated for the fabrication Ag/Cu_2O heterostructures. Ag/Cu_2O heterostructures exhibits enhanced photocatalytic activity under visible-light irradiation. Siyuan, *et al.* [**19**] $Ag–Cu_2O$ nano-composites have been controllably prepared by a simple synthesis. $Ag–Cu_2O$ with suitably exposed Ag surface shows much higher photocatalytic activity. Shouqiang, *et al.* [**20**] Ag/Cu_2O films have been fabricated using a facile method. Photocatalytic activity of Ag/Cu_2O films is higher than that of Cu_2O. Ag is well-known for its intense interactions with visible-light via the resonance of the oscillations of the free electrons within the particles [**21**], and is considered as a relatively cheap noble metal. Photo excited electrons in the conduction band (CB) of a semiconductor can be transferred to the noble metals, which act as electron sinks due to the Schottky barrier at the metal−semiconductor interface, while the holes can remain on the semiconductor surface [**22, 23**]. The recombination of electrons and holes can therefore be prolonged, and the photocatalytic activity will be improved [**24**]. In addition, the plasmon resonance of noble metal nanoparticles (NPs) is expected to enhance absorption of incident photons, which will enhance the photocatalytic efficiency of the semiconductors [**25**]. Therefore, it is postulated that Cu_2O nanospheres modified with Ag particles may exhibit an enhanced photocatalytic activity.

Herein the synthesis of Cu_2O and $Ag\text{-}Cu_2O$ nanoparticles via reflux method using citric acid and EDTA. The prepared NPs were characterized using powder X-ray diffraction (PXRD), Fourier transform infrared analysis (FTIR), UV-diffused reflectant spectrum (UVDRS), scanning electron microscopy (SEM) and transmission electron microscopy (TEM) of the Cu_2O NPs. Photocatalytic activity of Cu_2O was examined by photodegradation of methylene blue (MB) under visible light illumination and photoluminescence (PL) study was also carried out.

Experimental

Synthesis of Cu_2O by reflux method using EDTA

100 mL of 10 mM copper nitrate solution, 3.4 mM EDTA and 34 mg of PVP was mixed and stirred for 30 minutes. 10 mL of NaOH (2M) was added drop wisely. The solution is again stirred for 30 minutes. The resulting solution was mixed with 10 mL of ascorbic acid as a reducing agent and heated the solution for 2 hours at 70°C. The obtained product was washed with water followed by methanol and dried.

Characterization

The synthesized nanoparticles were characterized by using powder X-ray diffractometer (Rigaku Smart Lab). FTIR (Bruker-alpha) to analyze metal oxide bond stretching frequencies. The UV- DRS spectrum of the NPs was measured using UV-Visible spectro-photometer (Lab India-Diffuse reflectance spectra and Cary 60 Agilent technologies-Absorbance spectra). The morphologies of the prepared nanoparticles were scanned using Scanning Electron Microscopy (Hitachi-7000 Table top). Shape and size of the Cu_2O crystallites was determined using transmission electron microscope (JEOL 3010). Photoluminescence studies were recorded using fluorescence spectrophotometer Agilent Technology Cary Eclipse).

Photocatalytic activity

Photo-Reactor "Heber" was purchased from Chennai. The photocatalytic reactor consists of a medium pressure mercury vapor lamp (λ max = 365 nm, 250W) in a jacketed quartz crystal tube. The heat caused by the lamp was removed from cold water by continuous circulation throughout the jacket. The tube has an inside diameter of 2.3 cm, with an outer diameter of 2.7 cm diameter, which is 37 cm long, 100 ml capacity and is placed around the lamp.

The gap between the mercury lamp and the quartz tube containing pollutant was 6 cm. The uniform distribution of catalytic particles throughout the solution was achieved using air pump [**26**]. The solution was allowed for constantly bubbled in the dark for 30 minutes to ensure the organization of an adsorption-desorption equilibrium between the photocatalyst and MB previous to irradiation of light source. The

suspension 2 mL was withdrawn from the reactor over 30 minutes intervals. Centrifuge the solution using spin win microcentrifuger to remove the Cu_2O NPs from the mixture. The dye concentration of left-over aqueous solution was measured using UV-Vis spectro-photometer at 664 nm. The % degradation of the MB is calculated using the equation (i)

$$\% \text{ of degradation} = \frac{Ci - Cf}{Ci} \times 100 \quad (1)$$

where C_i initial and C_f final dye concentrations in ppm. The photocatalytic experiment was repeated by changing different parameters such as concentration of dye, catalytic load, pH variation, catalyst recycling, etc.

Result and discussion

PXRD study

The PXRD patterns of Cu_2O nanoparticles are represented in **Fig. 1**. From the XRD data indicated that Cu_2O NPs has cubic phase structure and space group Pn-3m resemble with the standard JCPDS card number 1-1142 [**27**]. No extra peaks were found in the pattern which indicates that purity of the samples. The average crystallite size was measured to be 9.5 nm for Cu_2O and 7.5 nm for Ag-Cu_2O, respectively.

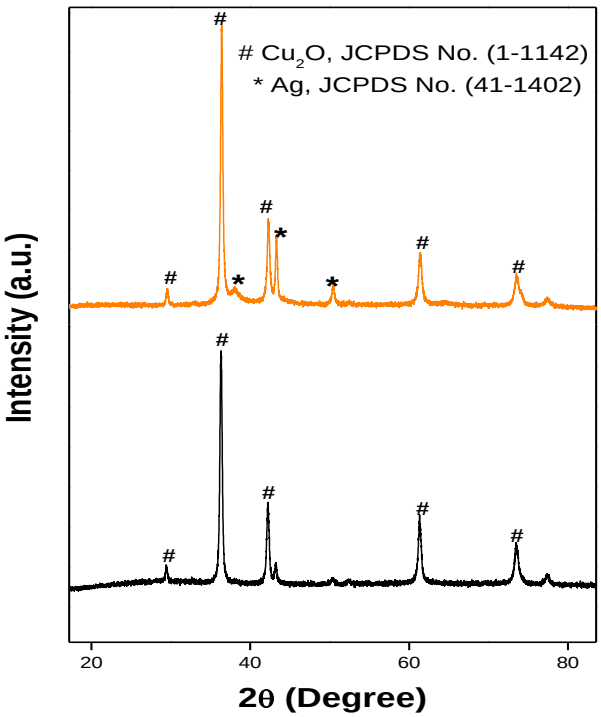

Fig. 1. Powder XRD patterns of Cu_2O and Ag-Cu_2O nanoparticles.

FTIR study

The FTIR spectra of Cu_2O and Ag-Cu_2O nanomaterials were recorded between the ranges of 4000 to 400 cm^{-1} as shown in **Fig 2**. Additionally, characteristic bands of Cu_2O, which include the Cu-O symmetric and asymmetric stretching vibrations at 630 cm^{-1} were also observed [**28**]. The broad peak at 3413 and 1619 cm^{-1} is due to the stretching and bending vibrations of -OH, which is due to the absorbed moisture on the surface of the catalyst [**29, 30**].

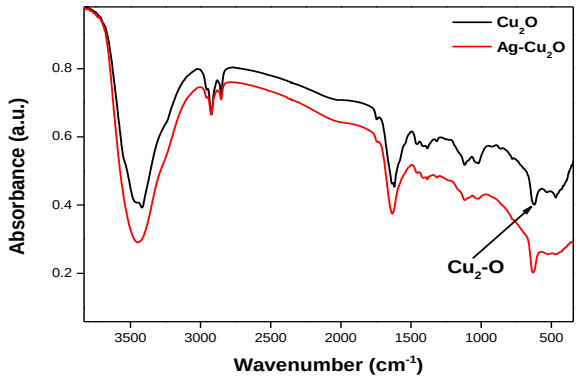

Fig. 2. FTIR spectra of Cu_2O and Ag-Cu_2O nanoparticles.

UV-Visible Diffuse reflectance studies: (UV-DRS)

Fig. 3 shows the UV–Visible spectra of Cu_2O and Ag-Cu_2O NPs synthesized by EDTA. The spectra demonstrate with absorption band shown nearly at 490 to 510 nm. Due to electron transfer from valence band to conduction band. The calculated Eg values were found to be 2.4 eV and 2.3 eV for Cu_2O and Ag-Cu_2O NPs respectively [**31**].

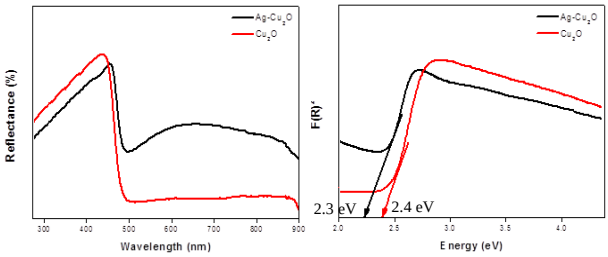

Fig. 3. UV-DRS spectra of Cu_2O and Ag-Cu_2O nanoparticles.

Scanning Electron Microscopy (SEM) studies

Fig. 4 (a, b) represents SEM images of the compound Cu_2O and **Fig. 4 (c, d)** for Ag- Cu_2O NPs. The particles are looking like a cube like structures, which are formed by the agglomeration of NPs. The single layered cubes like structures are visible from the SEM images.

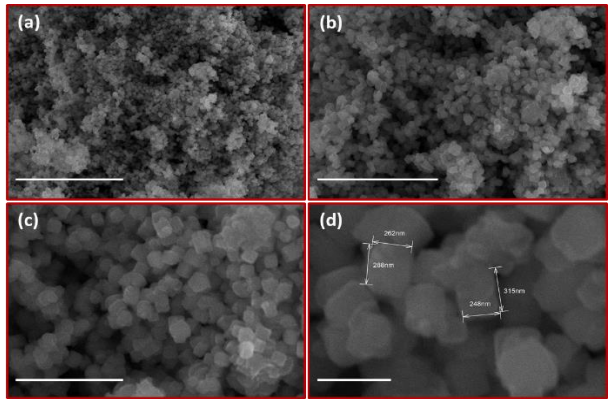

Fig. 4. SEM images of Cu_2O nanomaterials (a) and (b), and Ag-Cu_2O nanomaterials (c) and (d).

Transmission Electron Microscopy (TEM) studies

Fig. 5 shows the TEM images, HR-TEM.images and SAED pattern of synthesized Ag-Cu_2O NPs using EDTA via reflux method. From the TEM images (**Fig. 5a, b**) we can clearly observe the fine distribution of silver (Ag) on cube like Cu_2O nanomaterials. In the **Fig. 5c**. The distributed silver (yellow colored mark) on Cu_2O acquired spherical shape with size of 5.22 to 19.3 nm. The sizes of Cu_2O cubes (red colored mark) were observed 62.08 to 88.42 nm. From the SAED pattern, (**Fig. 5d**) it is confirmed as a polycrystalline in nature due to the diffracted spots are combined together to form a fringe of circles and these circles are well matched with the d-spacing values and planes calculated from XRD data. The planes at (110), (111) and (200) planes having highest intensity in XRD and which are matched with bright circular fringes in SAED pattern. From the **Fig. 5e**, it is confirmed that the size of the Ag nanoparticles was present in the range of 5 to 20 nm and 70 % distribution was observed for 15 to 17 nm sized particles. From the **Fig. 5f**, it is confirmed that the size of the Cu_2O nanoparticles were present in the range of 60 to 80 nm and 68 % distribution was observed for 75 to 80 nm sized particles.

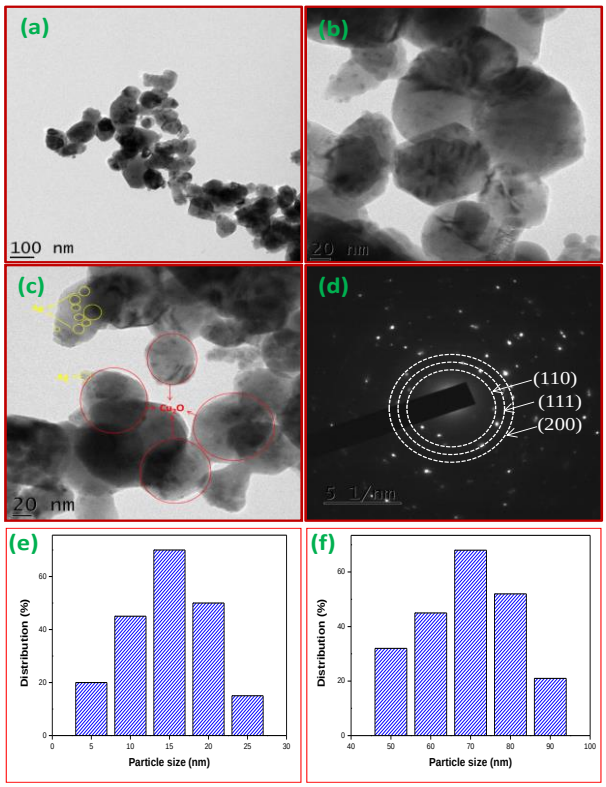

Fig. 5. TEM images (a,b), HR-TEM images (c) and SAED pattern (d) of Ag-Cu_2O nanomaterials, (e) distribution of Ag on Cu_2O, (f) distribution of Cu_2O.

Photocatalytic degradation of Cu_2O and Ag-Cu_2O NPs

Under light radiation, the semiconductor absorbs photons of energy greater than the band gap of semiconductors and then creates electrons and holes in the valence and conducting band. If the charge carriers don't accompanied, then they'll travel on the surface wherever free electrons form the reduction of oxygen and form the peroxides and superoxides and created holes oxidize the water and form the OH·; these generated species are extremely reactive and unstable and ultimately cause to the degradation of organic dyes.

Many factors are influencing the Photocatalytic action on dyes, i.e., band gap, surface area, crystallinity, phase composition, surface hydroxyl density, size distribution, morphology, and particle size of the photocatalyst [**32**]. Prepared Cu_2O NPs were taken as photocatalyst to check the methylene blue dye degradation under UV-light. In every 30 minutes, 2mm of the aliquots sample solution was withdrawn and it was centrifuged and absorption of the samples was recorded. By measuring the change in intensity, we can calculate the degradation rate of dye at λ max-664 nm.

Effect of dye concentration

The concentration of the dye is playing a crucial role in photocatalytic activity of Cu_2O nanomaterials. Hence, so as to judge the optimum concentration of dye for promising photocatalytic activity, the experiment was carried out by changing the dye concentration of 5-20 ppm under catalytic loading constant (100 mg) and UV light as in **Fig. 6**.

This clearly shows that as the dye concentration of 5-20 ppm increases, the photocatalytic degradation is reduced by 80-20% and 5 ppm is the most effective concentration for dye degradation. Generally, as increases the dye concentration, the number of dye molecules is adsorbed on the surface of Cu_2O nanoparticles, so the degradation rate decreases. On the other hand, adsorbed dye molecules were not degraded more rapidly because of the constant light intensity and catalyst loading.

The higher the dye concentration, the smaller the penetration power of light, which means that the photocatalytic decomposition is less at higher concentrations with less occurrence of hydroxyl groups and superoxide radicals [**33**].

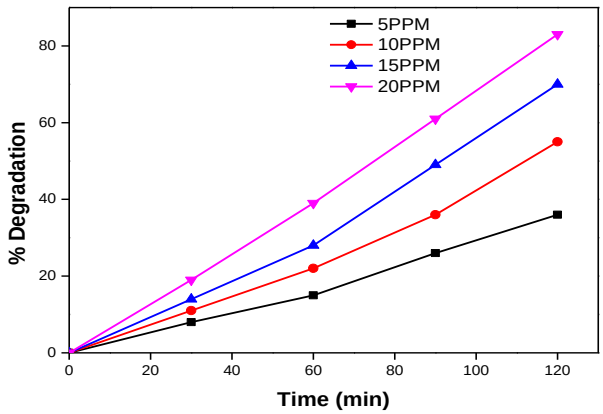

Fig. 6. Degradation MB with varying concentration of dye constant and catalyst load constant.

Effect of catalytic load

Fig. 7 represents the graph of MB degradation with varying catalyst load (5-20 mg) by maintaining the constant concentration of dye (100 mL of 5 ppm). The data clearly reveals that as the catalyst load increases over 120 minutes, the rate of dye degradation increases from 80% to 100%. This is because more active sites are available due to increased catalytic load [**33**].

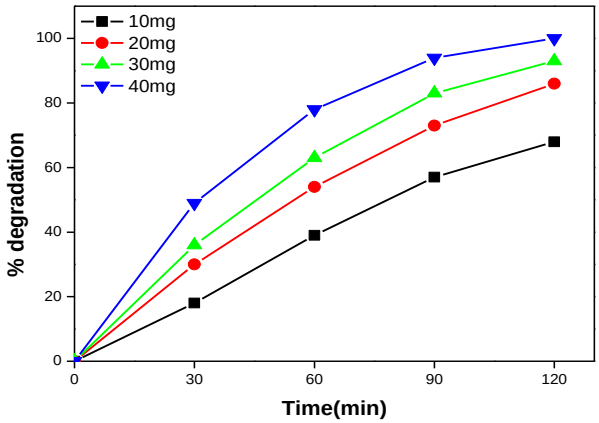

Fig. 7. Degradation of Methylene Blue with varying catalyst load and constant dye concentration.

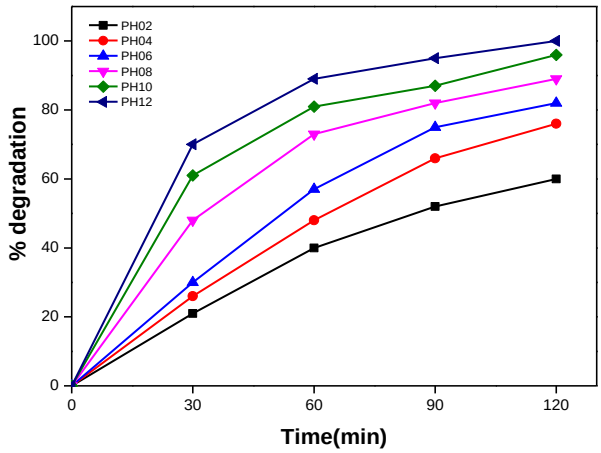

Fig. 8. Degradation of MB with varying pH of the solution and keeping the catalyst load and constant dye constant.

Effect of pH

In order to see the optimum pH for the photolysis of the MB dye, experiments were conducted at completely different pHs (2 to 12) by maintaining the constant catalyst (100 mg) and the dye concentration (5 ppm), and the result represented in **Fig. 8**. This clearly shows that the MB degradation was effective in the basic medium [**34, 35**] with the very best degradation rate at pH 10. On top of this pH the degradation decreases, which may be explained on the basis of zero potential charge. The presence of a large number of OH^- ions on the surface of the catalyst can produced less range of $OH^{\bullet}$ radicals, that act as primary oxidizing agents and are responsible for the degradation of MB dye [**36-40**].

Kinetics of photocatalytic degradation

The obtained results of photocatalytic activity of Cu_2O and Ag-Cu_2O NPs were explained through kinetic study using Langmuir–Hinshelwood model. The photodegradation of MB dye as presented in the following relation

$$\ln(C_0/C_t) = kt \quad (2)$$

where, C_0 is the initial concentration of dye (mg/L) at t = 0, C_t is the concentration after irradiation in the selected time interval (30 min), k is the rate constant. The plots of ln (Co/Ct) as a function of reaction time which is approximate. From **Fig. 9**. The slopes of the straight lines from the plot of ln (Co/Ct) vs reaction time are the rate constants (k) for photocatalytic degradation of MB for Cu_2O and Ag- Cu_2O NPs. The rate constant k has the highest value for Ag-Cu_2O NPs was 0.5×10^{-2} min^{-1} compared to Cu_2O which was 0.3×10^{-2} min^{-1} under visible light illumination [**41**].

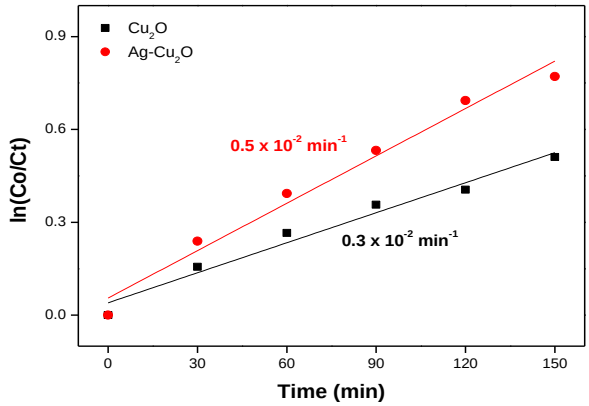

Fig. 9. Photocatalytic kinetic studies of Cu_2O and Ag-Cu_2O NPs.

Catalyst recycling

To evaluate the stability of the photocatalyst, a recycling experiment was carried out to degradation the methylene blue dye (**Fig. 10**). The experiment was carried out with 100 mg of catalyst and 100 ml of 5 ppm dye. The decomposition potency of MB was nearly an equivalent for six cycles. This figure clearly shows a reduction in potency of nearly 80% altogether six cycles.

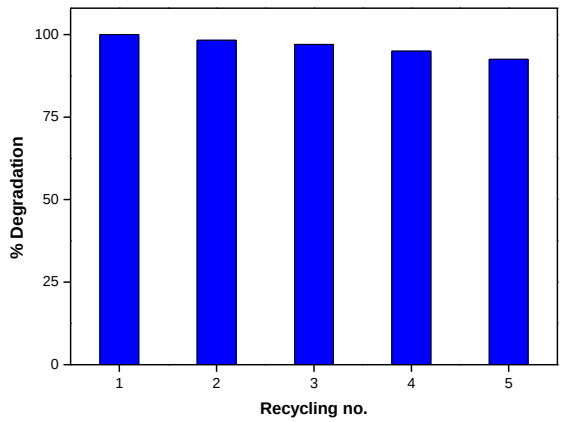

Fig. 10. Recycling of 10 mg of catalyst and 100 ml of 5 ppm dye.

Mechanism scheme

A schematic representation of the degradation of MB using Cu_2O superstructure is shown below.

$Cu_2O + h\nu \rightarrow Cu_2O (h^+_{vb} + e^-_{cb})$

$OH^-_{ads} + h^+_{vb} \rightarrow OH^{\bullet}_{ads}$ (in basic medium)

$MB + OH^{\bullet}_{ads} \rightarrow$ dye degradation

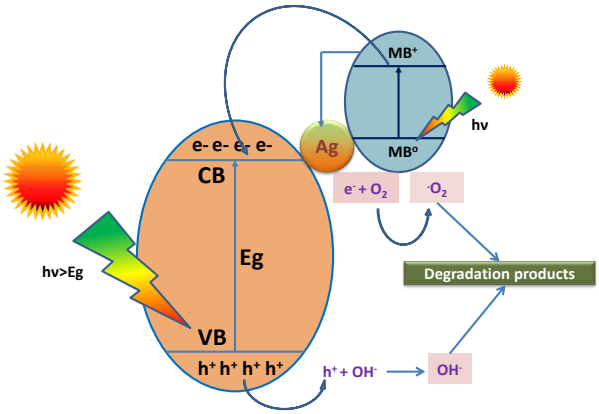

Mechanism. 1. Graphical representation for the mechanism of Cu_2O under the irradiation of UV light.

Detection of OH· radicals

$OH^{\bullet}$ radicals are the most reactive species throughout photocatalytic degradation reactions. The rate of $OH^{\bullet}$ formation and detection can be measured with straight forward, sensitive and quick PL (photoluminescence) techniques using coumarin as the probe molecule. $OH^{\bullet}$ reacts with coumarin to produce a fluorescent compound 7-hydroxyl coumarin at 456 nm.

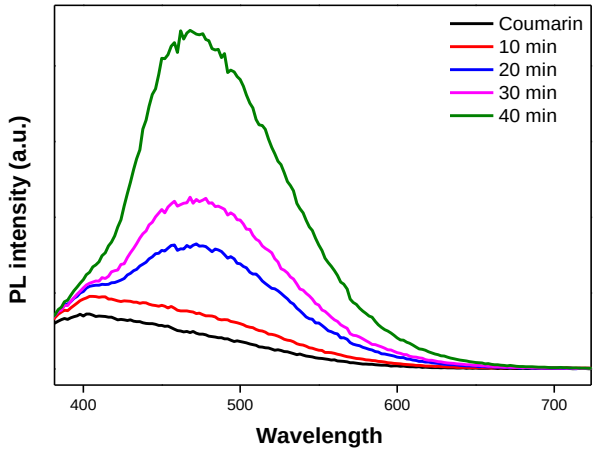

Fig. 11. Concentration of hydroxyl radicals against irradiation time.

In this method, Cu_2O (130 mg) was dispersed in 1 mM coumarin (50 mL) aqueous solution was taken in borosil jar. The solution mixture was allowed to stand for 10 minutes to attain adsorption-desorption equilibrium between Cu_2O, water and coumarin before irradiation. This reaction was irradiated with ultraviolet light of 60 W capacity as a light source. Aliquots of 2 milliliters were collected each ten minutes and the PL spectra were measured using an Agilent Technologies Cary Eclipse spectrophotometer. **Fig. 11** shows that the PL intensity at 531 nm will increases linearly with time and clearly indicates that the formation of OH on the Cu_2O surface is directly proportional to the irradiation time [**42**]. It shows that formation of $OH^{\bullet}$ increases with an increase in time. This $OH^{\bullet}$ is liable for the decomposition of organic dyes.

Photoluminescence studies

PL study is one among the helpful technique for notice the potency of charge carrier separation within the semiconductor **[43]**. The PL emission spectrum of Cu_2O and Ag-Cu_2O NPs were recorded in room temperature with an excitation wavelength of 250 nm represented in **Fig. 12a**. The pure Cu_2O Nps provides a strong ultraviolet emission peak at 712 nm and weak emission peak at 564 nm. In case of Ag-Cu_2O Nps, the obtained PL emission intensity decreased and the resultant data are in good agreement with the Stern-Volmer quenching.

This indicates the efficiency of high charge carrier separation in Ag-Cu_2O NP_S. The emission peaks in visible region can be ascribed to bound excitons and defect states positioned at surface of nanostructured pure and doped Cu_2O Nps respectively. Chromaticity coordinates are used to find luminous colored objects and it can be estimated by Commission International De I'Eclairage (CIE) system. CIE chromaticity diagram of Cu_2O and Ag-Cu_2O Nps represented in **Fig. 12b** reveals that both the material emits yellow light region [**44, 45**].

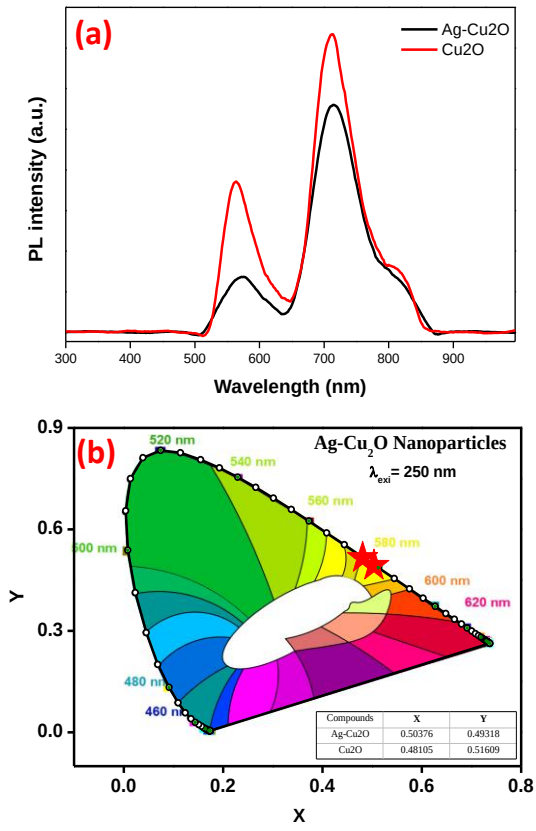

Fig. 12. PL spectrum of Cu_2O and Ag-Cu_2O (a) emission spectra (b) CIE diagram (c) CIE diagram.

Conclusion

In this study, Cu_2O and Ag-Cu_2O nanoparticles were prepared by employing reflux method using EDTA. The XRD pattern shows that Cu_2O and Ag-Cu_2O nanoparticles belong to a cubic phase with an average crystallite size of 9.5 nm and 7.5 nm respectively. The SEM image clearly shows that the cube like structures of Cu_2O. The TEM image shows that the particles are virtually agglomerated and crystalline. The prepared Cu_2O and Ag-Cu_2O NPs display 80 to 90 % photodegradation activity over methylene blue dye. The photoluminescence study reveals that Cu_2O and Ag-Cu_2O nano particles shown yellow color emission.

Acknowledgement

Mr. Udayabhanu gratefully acknowledge CSIR, New Delhi, for financial support through SRF (09/1204(0001)2018-EMR-I). Dr. GN thanks DST-Nanomission (SR/NM/NS-1262/2013) for financial support. Mr. Basavalingaiah thanks SIT for providing lab facilities.

References

1. Fox, M. A.; Dulay, M. T., *Chem. Rev.*, **1993**, *93*, 341.
2. Fujishima, A., *Nature*, **1972**, *238*, 37.
3. Li, Y.; Fang, X.; Koshizaki, N.; Sasaki, T.; Li, L.; Gao, S. Y.; Shimizu, Y.; Bando, Y.; Golberg, D., *Adv. Funct. Mater.*, **2009**, *19*, 2467.
4. Qiu, Y.; Yan, K.; Deng, H.; Yang, S. H., *Nano Lett.*, **2011**, *12*, 407.
5. Lu, C. H.; Qi, L. M.; Yang, J. H.; Wang, X. Y.; Zhang, D. Y.; Xie, J. L.; Ma, J. M., *Adv. Mater.*, **2005**, *17*, 2562.
6. Zheng, Z.; Huang, B. B.; Wang, Z. Y.; Guo, M.; Qin, X. Y.; Zhang, X. Y.; Wang, P.; Dai, Y., *J. Phys. Chem. C.*, **2009**, *113*, 14448.
7. Zhang, Y.; Deng, B.; Zhang, T. R.; Gao, D. M.; Xu, A. W., *J. Phys. Chem. C.*, **2010**, *114*, 5073.
8. Ma, L. L.; Li, J. L.; Sun, H. Z.; Qiu, M. Q.; Wang, J. B.; Chen, J. Y.; Yu, Y., *Mater. Res. Bull.* **2010**, *45*, 961.
9. Hu, C. C.; Nian, J. N.; Teng, H., *Sol. Energy Mater. Sol. Cells*, **2008**, 92, 1071.
10. Siripala, W.; Ivanovskaya, A.; Jaramillo, T. F.; Baeck, S. H.; McFarland, E. W. A., *Sol. Energy Mater. Sol. Cells*, **2003**, *77*, 229.
11. Huang, L.; Peng, F.; Wang, H.; Yu, H.; Li, Z., *Catal. Commun.*, **2009**, *10*, 1839.
12. Gajengi, A. L.; Fernandes, C. S.; Bhanage, B. M., *Mol. Cat.*, **2018**, *451*, 13.
13. Wang, Z.; Zhao, S.; Zhu, S.; Sun, Y.; Fang, M., *Cryst. Eng. Comm.*, **2011**, *13*, 2262.
14. Wang, L.; Qi, H.; Chen, L.; Sun, Y.; Li, Z., *Nanomaterials*., **2018**, *8*, 332.
15. Sasmal, A. K.; Pal, J.; Sahoo, R.; Kartikeya, P.; Dutta, S.; Pal, T., *J. Phys. Chem. C.*, **2016**, *120*, 21580.
16. Zhang, W.; Yang, X.; Zhu, Q.; Wang, K.; Lu, J.; Chen, M.; Yang, Z., *Indus. Eng. Chem. Res.*, **2014**, *53*, 16316.
17. Yang, J.; Li, Z.; Zhao, C.; Wang, Y.; Liu, X., *Mat. Res. Bull.*, **2014**, *60*, 530.
18. Sun, Y.; Cai, L.; Liu, X.; Cui, Z.; Rao, P., J. Phy. Chem. Sol., **2017**, *111*, 75.
19. Yang, S.; Zhang, S.; Wang, H.; Yu, H.; Fang, Y.; Peng, F., *Mat. Res. Bull.*, **2015**, *70*, 296.
20. Wei, S.; Shi, J.; Ren, H.; Li, J.; Shao, Z., *J. Mol. Catal. A: Chem.*, **2013**, *378*, 109.
21. Peng, S. J.; Li, L. L.; Tan, H. T.; Wu, Y. Z.; Cai, R.; Yu, H.; Huang, X.; Zhu, P. N.; Ramakrishna, S.; Srinivasan, M.; Yan, Q. Y., *J. Mater. Chem. A.*, **2013**, *1*, 7630.
22. Hoffmann, M. R.; Martin, S. T.; Choi, W. Y.; Bahnemann, D. W., *Chem. Rev.* **1995**, *95*, 69.
23. Li, X. Z.; Li, F. B., *Environ. Sci. Technol.* **2001**, *35*, 2381.
24. Pan, Y. L.; Deng, S. Z.; Polavarapu, L.; Gao, N. Y.; Yuan, P. Y.; Xu, C. H., *Langmuir.*, **2012**, *28*, 12304.
25. Schaadt, D. M.; Feng, B.; Yu, E. T., *Appl. Phys. Lett.*, **2005**, *86*, 063106.
26. Phattepur, H.; Siddaiah, G. B.; Ganganagappa, N., *Perio. Polytech. Chem. Eng.*, **2019**, *63*, 85.
27. Song, S.; Yang, H.; Zhou, C.; Cheng, J.; Jiang, Z.; Lu, Z.; Miao, J., *Chem. Eng. Journal.*, **2017**, *320*, 342.
28. García-Pérez, U. M.; Sepúlveda-Guzmán, S.; Martínez-De La Cruz, A., *Solid State Sci.*, **2012**, *14*, 293.
29. Hower, P.; Gupta, T., *J. Appl. Phy.*, **1979**, *50*, 4847.
30. Wahab, R.; Ansari, S.G.; Kim, Y.S.; Seo, H.K.; Kim, G.S.; Khang, G.; Shin, H.S., *Mat. Res. Bulletin.*, **2007**, *42*, 1640.
31. Udayabhanu.; Nagaraju, G.; Nagabhushana, H.; Basavaraj, R.B.; Raghu, G.K.; Suresh, D.; Rajanaika, H.; Sharma, S.C., *Crys. Growth & Design.*, **2016**, *16*, 6828.
32. Suresh D.; Nethravathi, P.C.; Udayabhanu.; Rajanaika, H.; Nagabhushana, H.; Sharma, S.C.; *Mat. Sci. Semicond. Proces.*, **2015**, *31*, 446.
33. Suresh D.; Nethravathi, P.C.; Lingaraju, K.; Rajanaika, H.; Sharma, S.C.; Nagabhushana, H., *Spectro. Acta Part A: Mole. Biomol. Spectro.*, **2015**, *136*, 1467.
34. Madan, H. R.; Sharma, S. C.; Suresh, D.; Vidya, Y. S.; Nagabhushana, H.; Rajanaik, H.; Maiya, P. S., *Spectro. Acta Part A: Mole. Biomol. Spectro.*, **2016**, *152*, 404.
35. Khodja, A.A.; Sehili, T.; Pilichowski, J.F.; Boule, P., *J. Photochem. Photobio. A: Chem.*, **2001**, *141*, 231.
36. Anandan, S.; Vinu, A.; Lovely, K.S.; Gokulakrishnan, N.; Srinivasu, P.; Mori, T.; Murugesan, V.; Sivamurugan, V.; Ariga, K., *J. Mole. Catal. A: Chemical.*, **2007**, *266*, 149.
37. Poulios, I.; Tsachpinis, I., *J. Chem. Tech. Biotech.: Inter. Res. Process, Environ. & Clean Tech.*, **1999**, *74*, 349.
38. Liqiang, J.; Xiaojun, S.; Baifu, X.; Baiqi, W.; Weimin, C.; Honggang, F., *J. Sol. State Chem.*, **2004**, *177*, 3375.
39. Mills, A.; Davies, R.H.; Worsley, D., *Chem. Soc. Rev.*, **1993**, *22*, 417.
40. Rengaraj, S.; Li, X.Z., *Inter. J. Envir. Poll.*, **2006**, *27*, 20.
41. Lassoued, A.; Lassoued, M.S.; Dkhil, B.; Ammar, S.; Gadri, A., *J. Mat. Sci.: Mat. Electro.*, **2018**, *29*, 7057.
42. Xiang, Q.; Yu, J.; Wong, P.K., *J. Coll. Inter. Scie.*, **2011**, *357*, 163.
43. Nagaraju, G.; Nagabhushana, H.; Suresh, D.; Anupama, C.; Raghu, G.K.; Sharma, S.C., *Ceram. Inter.*, **2017**, *43*, 11656.
44. Nagaraju, G.; Prashanth, S.A.; Shastri, M.; Yathish, K.V.; Anupama, C.; Rangappa, D., *Mat. Res. Bulletin.*, **2017**, *94*, 54.
45. Basavalingaiah, K.R.; Udayabhanu.; Harishkumar, S.; Nagaraju, G.; Chikkahanumantharayappa; *Asian J. Engi. Appl. Tech.*, ***2019,*** *8*, 79.

